



Lamb wave-based damage localization and quantification algorithms for CFRP composite structures

Xianping Zeng, Xiao Liu, Jiajia Yan, Yinghong Yu, Bowen Zhao, Xinlin Qing^{*}

School of Aerospace Engineering, Xiamen University, Xiamen, Fujian 361005, PR China

ARTICLE INFO

Keywords:
 Composite structure
 Damage monitoring
 Lamb wave signal
 Quantitative damage size

ABSTRACT

Accurately and quantitatively monitoring the damages in complicated composite structures is very challenging, but essential for assessing their integrity. In this paper, an innovative damage monitoring method based on Lamb wave is proposed for large-scale complicated composite laminates. A combination of a resource-constraint Levenberg-Marquardt algorithm associated with a quantum-inspired gravitational search algorithm is introduced to identify the damage location. A damage contour algorithm using convex envelope of damage reflection points and maximum inscribed n-polygon is developed to determine the quantitative damage size. Meanwhile, a singular loci removal scheme based on an automatically updated boundary region constraint and bivariate normal distribution is utilized to separate the correctly positioned points on the damage periphery from those associated with noise. Experiments on two large-scale composite panels with multiple damage cases are conducted to substantiate the proposed algorithms. Sensor layers with embedded piezoelectric transducer (PZT) sensor networks mounted on the structures are employed to excite and receive Lamb wave signals because of their superiority of flexibility, electrical stability and apt for complex structures. The results demonstrate that the proposed technique is capable of pinpointing both location and size of the damage in the complicated composite structures.

1. Introduction

Carbon fiber reinforced plastic (CFRP) composite materials have been extensively used in aerospace and other industries because of their extraordinary mechanical and in-service peculiarities [1]. However, the existence and propagation of certain unexpected damages (i.e. delamination, matrix cracking, etc.) engendered during the fabrication process or in-service application will seriously deteriorate the material strength and even result in catastrophic accidents [2]. Structural health monitoring (SHM), an essential technology capable of monitoring structural integrity in real-time, has been committed to monitoring the health status of the composite structure. The piezoelectric transducer (PZT)-based Lamb wave methodology is considered as an encouraging and gripping candidate in SHM, which is applicable for almost indiscernible damage detection in composite structures [3,4]. Nevertheless, a comprehensive action of dispersive and multi-modal effects commonly induced distortion for Lamb wave signals, which makes damage location identification and size quantification sophisticated, especially in complicated composite structures.

Recently, many different imaging approaches have been developed to characterize the features of damage regions, including tomography imaging technique [5], time reversal-based imaging algorithm [6], probability-based diagnostic imaging (PDI) [7], delay-and-sum (DAS) method [8], and their improved algorithms [9–11]. For example, Liu et al. [9] introduced a weight-compensated PDI algorithm to realize damage localization for a stiffened composite panel. Shan et al. [10] adopted an extended DAS method to attain high localization accuracy for a large CFRP aircraft panel under multi-damage cases. Besides, the time of flight (ToF) based damage evaluation approaches are extensively used for composited laminates. Using the ToF and the known distance between the sensors, the damage position can be estimated by triangulation [12], elliptical loci method [13], and optimization algorithm for solving nonlinear equations [14]. The methods reviewed above are based on deterministic frameworks, while the uncertainties such as material properties, and environmental factors generally have a great impact on the prediction results. Nevertheless, the uncertainties were not taken into account in the above methods. Cantero-Chinchilla et al. [15] and Yan [16] investigated a Bayesian system identification theory

* Corresponding author.

E-mail address: xinlinqing@xmu.edu.cn (X. Qing).

and Particle filter method respectively to eliminate the impacts of uncertainty factors for damage detection. However, the studies only focused on damage localization, yet did not perform quantitative estimates of damage size. Accordingly, some researchers also sought out the correlation between damage indexes (DI) and related damage size using signal processing techniques, e.g. the wavelet transform [17], the spectral envelope [18], and the Bayesian estimator [19]. Hu et al. [20] deduced a mathematical relationship between the wave reflection intensity and the damage size for through-thickness circular holes by a numerical simulation. Qiu et al. [21] combined the DI and DAS methods for damage localization, and used a prior statistic model for quantitative monitoring. However, circumstances for Lamb wave signals to extract DI and build the relationships or the prior models generally discriminate from that the target structure undergoes. Recently, tremendous efforts have been made to explore the hidden damage characteristics in datasets by employing data-driven or machine learning techniques. Zhang et al. [22] and Wu et al. [23] adopted a convolutional neural network combined with signal processing techniques to conduct damage assessment. In literature [24], five machine learning approaches were performed to estimate the delamination area for CFRP composites. In addition, statistical modelling is also frequently used in the damage detection region [21]. Although artificial intelligence methods and statistical modelling can yield satisfactory results, they rely on a large amount of training data or statistical libraries, which are time-consuming and laborious.

Damage localization and quantification by determining the wave scattering sources with different sensing paths without priori information, which have been proverbially used in SHM. References [25–28] considered the most probable location of the wave scattering source in each sensing path as the reflection points on the damage boundary. The convex envelope of the identified reflection points is exploited to characterize the shape and size of the damage. However, the above researches mainly were carried out with metallic plates or only adopted from numerical simulation. Thus damage evaluation in complex composite structures remains a challenging subject that still needs to be studied.

Concerning the problems above, this paper focuses on developing an innovative damage location identification and size quantification method based on the Lamb wave for large-scale complicated composite structures. The damage location is obtained by solving a set of non-linear equations through a combination of a resource-constraint Levenberg-Marquardt (LM) algorithm associated with a quantum-inspired gravitational search algorithm (QGSA). With the simultaneous interpretation of the position of wave scattering sources from different sensing paths, the damage size can be estimated quantitatively. The convex envelope and maximum inscribed n-polygon techniques are implemented to characterize the size of the damage. Since the signals captured are usually polluted with noise, a singular elliptical loci removal scheme based on an automatically updated boundary region constraint and bivariate normal distribution, is used to separate the noise reflection points away from the damage estimation center. In addition, sensor layers with embedded PZT sensor networks mounted on the structures are utilized to generate and receive Lamb wave signals due to their extraordinary application performance [29]. Experiments on two large-scale composite panels with multiple damage cases are conducted to substantiate the proposed techniques.

The layout of this paper is as follows: Section 2 describes the details of damage assessment methodologies. Section 3 introduces the experimental validation performed on two composite panels with thirty-two different artificial and real damage cases. Section 4 summarizes the conclusion.

2. Methodology of damage assessment

2.1. Damage location identification

As shown in Fig. 1, an active sensor network consisting of N actuators

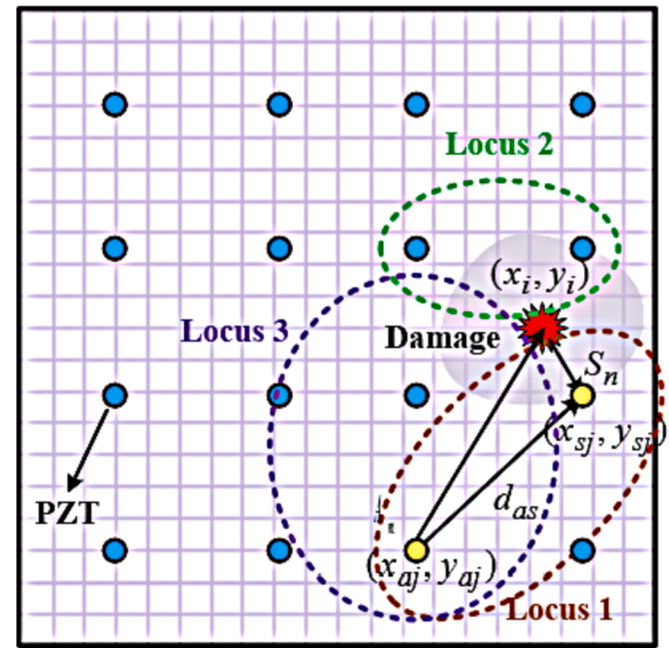


Fig. 1. Description of damage localization based on multiple elliptical loci.

and sensors in conformity to the pitch-catch A_m-S_n ($m, n = 1, 2, \dots, N$ but $m \neq n$) configuration, is schemed to capture signal characterizations associated with damage. The monitoring area can be firstly meshed into uniformly distributed grids. Supposing each node of the grids in the composite plate is a possible damage location, the probability of the presence of damage at each node (x_i, y_i) can be expressed as:

$$p(x_i, y_i) = \sum_{j=1}^{N_p} p_j(x_i, y_i) = \sum_{j=1}^{N_p} G_j \Gamma(T_{aj} + \Theta_j(x_i, y_i) \cdot (T_{bj} - T_{aj})) \zeta_j^{c(t)} \quad (1)$$

where.

$$\zeta_j^{c(t)} = \begin{cases} 1, & T_{aj} < t < T_{sj}^{TH} + \delta, \quad \Gamma(T_{sj}^{TH}) = \text{firstpeak}(\Gamma_j^{c(t)}) \\ 0, & \text{others} \end{cases} \quad (2)$$

$$\Theta_j(x_i, y_i) = \frac{\sqrt{(x_i - x_{aj})^2 + (y_i - y_{aj})^2} + \sqrt{(x_i - x_{sj})^2 + (y_i - y_{sj})^2}}{\sqrt{(x_{aj} - x_{sj})^2 + (y_{aj} - y_{sj})^2}} \quad (3)$$

$c(t)$ is the scattered signal that obtained by subtracting the baseline signal from the monitored signal containing the damage information. $\Gamma(\bullet)$ represents the envelope of the scattered signal $c(t)$, which can be extracted by the Hilbert transform. Assuming there are N_p sensing paths in total, $p_j(x_i, y_i)$ is the damage probability estimated from the j th sensing path. (x_{aj}, y_{aj}) and (x_{sj}, y_{sj}) are the coordinates of the actuator and sensor in the j th sensing path. G_j is signal amplification factor. T_{aj} is the time offset corresponding to the actuation, T_{bj} is the arrival time of a signal traveling from actuator (x_{aj}, y_{aj}) to sensor (x_{sj}, y_{sj}) . T_{sj}^{TH} is the time of the first peak extracted from the scattered signal envelope $\Gamma_j^{c(t)}$. δ is an empirical constant.

The locus of the possible damage location forms an ellipse with (x_{aj}, y_{aj}) and (x_{sj}, y_{sj}) as the foci, as shown the Locus 1 in Fig. 1. To determine the exact location of the damage from the infinite solution provided by the elliptical locus, it is necessary to have multiple sensing paths at different positions, e.g. Locus 2, Locus 3. However, for the large-scale complicated composite structures, using the entire sensor network usually bring large errors due to erroneous perceptions from certain singular loci. It is necessary to weaken the erroneous effect by constraining sensing resources. The distances between each sensor position

and the grid nodes contained in area $\Omega\{p(x_i, y_i) \geq k \cdot \max(p(x, y))\}$ are calculated using Euclidean distance. The sensors closest to each grid node are recorded and the number of sensors is counted as M_1 ($M_1 \leq N$), and the number of all sensing paths excited or received by these M_1 sensors is denoted by N_{pc} ($N_{pc} \leq N_p$). Only N_{pc} sensing paths excited or received by M_1 sensors which closest to the area $\Omega\{p(x_i, y_i) \geq k \cdot \max(p(x, y))\}$ are employed to realize damage localization. Thus, a set of nonlinear equations for the constrained sensor network can be constructed as follows:

$$\begin{cases} F(P(x, y)) = \Theta_j(x, y) \cdot (T_{bj} - T_{aj}) = T_{sj}^{TH}, j = 1, 2, \dots, N_{pc} \\ \text{s.t. } \Omega\{p(x_i, y_i) \geq k \cdot \max(p(x, y))\} \end{cases} \quad (4)$$

where $F(P(x, y))$ is a vector function with unknown positional parameters x and y . k is a parameter to control the size of the effectuate constrained region Ω . $p(x, y)$ is the damage probability matrix composed of all sensing paths.

Herein, an LM algorithm [30] with resource-constraints is introduced to solve the system of equations. In addition, a QGSA [31] is adopted to address the issue that LM algorithm affected by the initial value. The main steps using the improved LM algorithm (hereinafter referred to as QLMC algorithm) are given in Algorithm 1. The optimal solution P^+ is considered as the predicted most probable damage location.

Algorithm 1: QLMC modelling

```

Input: A vector function  $F(P(x, y))$ , a measurement vector  $T_s^{TH}$ , a constrained region  $\Omega$ .
Initialize  $N_s$  masses with random positions  $P_i^0$  ( $i = 1, 2, \dots, N_s$ ).
Output: A vector  $P^+ \in \mathbb{R}^\Omega$ , minimizing  $\|F(P(x, y)) - T_s^{TH}\|^2$ .
Algorithm:

K = 0; v = 2; J =  $\partial(F(P))/\partial P$ ; A =  $J^T J$ ;  $\epsilon_P = T_s^{TH} - F(P^0)$ ; g =  $J^T \epsilon_P$ ;
stop = ( $\|\epsilon_P\|_\infty \leq \epsilon_1$ )  $\mu = \tau * \max_{i=1,2}(A_{ii})$ ;
while (not stop) and ( $K < K_{\max}$ )
    forces  $F_{ij}^K = G^K(m_i^K \times m_j^K)(P_j^K - P_i^K)/(R_{ij}^K + \epsilon)$ 
    where gravitational coefficient  $G^K$ , mass  $m^K$ , distance  $R^K$ 
    acceleration  $a_i^K = (\sum_{j=1, j \neq i}^{N_s} \text{rand}_j \times F_{ij}^K) / m_i^K$ ;
    Gbest = argmin  $L(\text{best}_i)$ ;  $m_{\text{best}} = (1/N_s) \cdot \sum_{j=1}^{N_s} L(\text{best}_j)$ ;
     $q_i^K = (\text{rand}_i^1 \cdot L(\text{best}_i) + a_i^K \cdot Gbest) / (\text{rand}_i^2 + a_i^K)$ ;
    1 - 0.5K/K_{\max} \cdot P_i^K = q_i^K \pm b_i^K |m_{\text{best}} - P_i^{K-1}| \ln(1/\text{rand}_i^3);
    \text{if } F(P_i^K) < F(\text{best}_i) \text{, } L(\text{best}_i) = P_i^K;
    \text{if } F(L(\text{best}_i)) < F(Gbest) \text{, } Gbest = L(\text{best}_i);
    \text{if } Gbest \notin \Omega, Gbest = \text{boundary } \{\Omega\}_{\text{nearest}};
    \epsilon_P = T_s^{TH} - F(Gbest); g =  $J^T \epsilon_P$ ; stop = ( $\|\epsilon_P\|_\infty \leq \epsilon_1$ )  $K = K + 1$ ;
end

P = Gbest; K = 0;
while (not stop) and ( $K < K_{\max}$ )
    K = K + 1; solve( $(A + \mu I)\delta_P = g$ );
    if  $\|\delta_P\| \leq \epsilon_2 \|P\|$ , stop = true;
    else  $P_{\text{new}} = P + \delta_P$ ,  $\rho = (\|\epsilon_P\|^2 - \|F(P_{\text{new}}) - T_s^{TH}\|^2) / (\delta_P^T (\mu \delta_P + g))$ ;
    if  $\rho > 0$ ,  $P = P_{\text{new}}$  (if  $P_{\text{new}} \notin \Omega$ ,  $P_{\text{new}} = \text{boundary } \{\Omega\}_{\text{nearest}}$ );
    A =  $J^T J$ ;  $\epsilon_P = T_s^{TH} - F(P)$ ; g =  $J^T \epsilon_P$ ; v = 2;
    stop = ( $\|\epsilon_P\|_\infty \leq \epsilon_1$ )  $\text{or } (\|\epsilon_P\|^2 \leq \epsilon_3)$ ;  $\mu = \mu * \max(1/3, 1 - (2\rho - 1)^3)$ ;
    else  $\mu = \mu * v$ ; v =  $2^v$ ;
end
P+ = P.

```

2.2. Damage size estimation

When an elastic wave (e.g. Lamb wave) collides with damage, including hole, delamination, crack, etc., wave scattering would occur at the damage periphery. With the simultaneous interpretation of the locations of wave scattering sources for different actuator-receiver pairs, the damage size can be estimated quantitatively. The damage

quantitative assessment procedure consists of three stages to evaluate the severity of damages with a non-negligible size: preliminary identification of damage location, singular elliptical loci removal, and damage size quantification.

Assuming that the predicted most probable damage position is $P^+(x_e, y_e)$ shown in subsection 2.1. Each elliptical path locus with the shortest distance to $P^+(x_e, y_e)$ is supposed as the possible position of wave scattering sources. Fig. 2 indicates the diagram of elliptical loci reflected by the damage with a remarkable size. Points P_1 , P_2 and P_3 are three points on locus 1, 2 and 3 respectively, which with the shortest distance to the estimated damage centre $P^+(x_e, y_e)$. Since the Lamb wave signals are reflected from the damage periphery, using a further quantity of sensing paths would attain more reflection points, and the damage size can subsequently be characterized.

However, the signals captured are usually polluted with noise in reality, singular elliptical loci removal is a momentous step for quantitative damage assessment.

2.2.1. Singular elliptical loci removal scheme

Equation (4) indicates that inaccurate T_{sj}^{TH} would yield erroneous loci, and the application of these singular elliptical loci would result in certain reflection points being away from the actual damage periphery. Herein, automatically updated boundary region constraint and bivariate normal distribution are employed in the singular loci removal scheme. The schematic diagram of the proposed removal scheme can be exhibited in Fig. 3.

Only N_{qc} ($N_{qc} \leq N_p$) sensing paths excited or received by M_2 ($M_2 \leq N$) sensors which closest to the estimated position $P^+(x_e, y_e)$ are employed to realize damage size estimation. Firstly, Eq. (4) is used to obtain N_{qc} positioning loci, and the point set Ψ_1 with the shortest distance to the estimated damage center $P^+(x_e, y_e)$ on each locus is calculated. The initial threshold value of boundary constraint is set as $k_0 = k_0$, and $0 < k_0 < 1$, which can be obtained by empirical evaluation. Then the constrained region Ω is extracted. Thus point set Ψ_1 which characterizes the damage profile can be updated to the point set Ψ_2 .

$$\Psi_2 = \{\Psi_2 | \Psi_2 \in \{p(x_i, y_i) \geq k_0 \cdot \max(p(x, y))\}\} \quad (5)$$

The minimum convex hull containing the point set Ψ_2 is divided into uniformly distributed $L_x \times L_y$ grids. Suppose that the normal distribution functions along the X and Y axes are defined as $\bar{x}(\mu_x, \sigma_x^2)$ and $\bar{y}(\mu_y, \sigma_y^2)$ respectively, and then a bivariate normal distribution can be denoted as

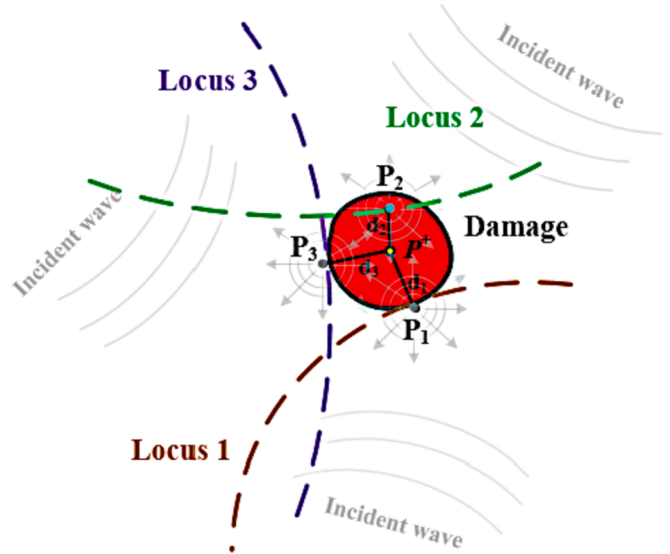


Fig. 2. Diagram of elliptical loci reflected by the damage with a non-negligible size.

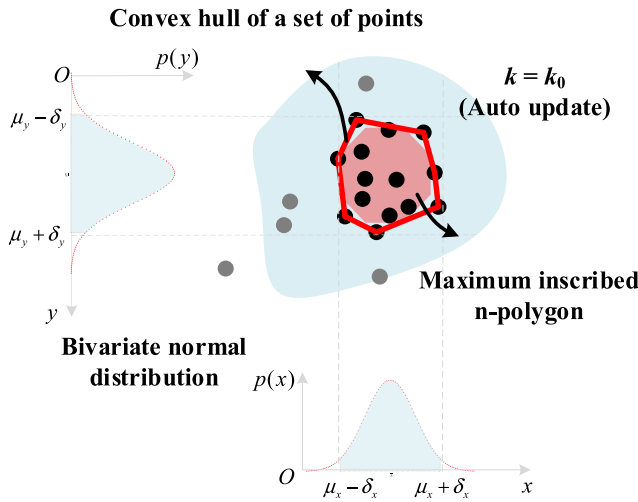


Fig. 3. Singular elliptical loci removal scheme: automatically updated boundary region constraint and bivariate normal distribution.

Eq. (6).

$$p(\bar{x}, \bar{y}) | \{\bar{x}, \bar{y} \in \Psi_2\} = \frac{1}{2\pi\sigma_x\sigma_y\sqrt{1-\rho_{xy}}} \exp \left[-\frac{\Phi}{2(1-\rho_{xy}^2)} \right] \quad (6)$$

where.

$$\Phi \equiv \frac{(\bar{x} - \mu_x)^2}{\sigma_x^2} - \frac{2\rho_{xy}(\bar{x} - \mu_x)(\bar{y} - \mu_y)}{\sigma_x\sigma_y} + \frac{(\bar{y} - \mu_y)^2}{\sigma_y^2} \quad (7)$$

and $|\rho_{xy}| < 1$ represents the correlation between \bar{x} and \bar{y} .

Then points located in the area with probability $p(\bar{x}, \bar{y})$ greater than δ_{xy} are retained, and the point set Ψ_2 can be updated to point set Ψ_3 .

$$\Psi_3 = \{\Psi_2 | \Psi_2 \in \{p(\bar{x}, \bar{y}) \geq \delta_{xy}\}\} \quad (8)$$

where δ_{xy} is an empirical constant that can be set to be linear with $\max\{p(\bar{x}, \bar{y})\}$.

Considering that the appropriate threshold value k of boundary constraint is critical for singular loci removal. In this study, a non-removal rate is employed to pick the suitable k .

Suppose that there are L_{Ψ_3} grids with probability $p(\bar{x}, \bar{y})$ greater than δ_{xy} . A non-removal rate Υ can be expressed as follows:

$$\Upsilon = L_{\Psi_3} / (L_x \times L_y) \quad (9)$$

If $\Upsilon \leq r_1$, it is necessary to enlarge the region Ω , that is, the threshold k should be reduced. If $\Upsilon \geq r_2$, region Ω needs to be narrowed, that is, k should be increased. Thus the point sets Ψ_2 and Ψ_3 are updated to point sets Ψ'_2 and Ψ'_3 respectively as follows:

$$\Psi'_2 = \{\Psi_1 | \Psi_1 \in \Omega \{p(x_i, y_i) \geq k_{update} \cdot \max(p(x, y))\}\} \quad (10)$$

$$\Psi'_3 = \{\Psi'_2 | \Psi'_2 \in \{p'(\bar{x}, \bar{y}) \geq \delta_{xy}\}\} \quad (11)$$

where k_{update} indicates the updated threshold. r_1 and r_2 are empirical constants.

Stop updating k until $r_1 < \Upsilon < r_2$. The newly updated point set Ψ'_3 is utilized to characterize the damage size.

2.2.2. Damage size quantification

The convex hull of the identified reflection point set Ψ'_3 is employed to characterize the damage size, and a convex combination of N_{Ψ} points $P_1, P_2, \dots, P_{N_{\Psi}}$ is a linear combination of the form.

$$C \equiv \left\{ \sum_{s=1}^{N_{\Psi}} \eta_s P_s \right\}, \text{ s.t. } \forall s : \eta_s \geq 0 \text{ and } \sum_{s=1}^{N_{\Psi}} \eta_s = 1 \quad (12)$$

where η_s is a weight assigned to each reflection point.

The damage contour is estimated by connecting all vertexes of the convex envelop, and then the damage size can be quantified by area calculation of the minimum convex polygon.

For the damage with an unknown shape, the damage size can be roughly estimated by the aforementioned convex hull method. Whereas for the damage with known shape, the accuracy of quantitative damage assessment can be further improved by calculating the maximum inscribed n - polygon, as shown in Fig. 3. Since the circle and rectangle can cover the most damaged shapes [25], the theories that quantified the size of circle-like or rectangle-like damage are introduced in this manuscript.

Suppose the polygon solved by convex hull C contains ξ sides and the coordinates of the endpoints are $(x_i, y_i), i = 1, 2, \dots, \xi$.

For circle-like damage, the damage radius R can be deduced as follows:

$$\max R \quad (13)$$

$$\text{s.t. } \begin{cases} 0 \leq R \leq d(x_c, y_c, x_i, y_i, x_{i+1}, y_{i+1}), i = 1, 2, \dots, \xi \\ R \leq (\max(x_i) - \min(x_i))/2, R \leq (\max(y_i) - \min(y_i))/2 \\ \text{point}(x_c, y_c) \in C \end{cases} \quad (14)$$

where point (x_c, y_c) is the central coordinate of the inscribed circle. Suppose a linear equation l composed of two adjacent endpoints (x_i, y_i) and (x_{i+1}, y_{i+1}) is expressed as $\kappa_1 x + \kappa_2 y + \kappa_3 = 0$. Draw a line passing through the point (x_c, y_c) and perpendicular to line l , the pedal coordinate (x_d, y_d) is given as

$$x_d = \frac{\kappa_2^2 x_c + \kappa_1 \kappa_2 y_c - \kappa_1 \kappa_3}{\kappa_1^2 + \kappa_2^2}, y_d = \frac{\kappa_2^2 y_c + \kappa_1 \kappa_2 x_c - \kappa_2 \kappa_3}{\kappa_1^2 + \kappa_2^2} \quad (15)$$

Thus, if (x_d, y_d) is on the line segment between (x_i, y_i) and (x_{i+1}, y_{i+1}) , then $d = (\kappa_1 x_c + \kappa_2 y_c + \kappa_3)/\sqrt{\kappa_1^2 + \kappa_2^2}$. But if not, $d = \min\left\{\sqrt{(x_c - x_i)^2 + (y_c - y_i)^2}, \sqrt{(x_c - x_{i+1})^2 + (y_c - y_{i+1})^2}\right\}$.

It should be noted that when $i = \xi$, the first constraint of Eq. (14) is modified as.

$$0 \leq R \leq d(x_c, y_c, x_i, y_i, x_1, y_1), i = 1, 2, \dots, \xi \quad (16)$$

For rectangle-like damage, the damage size can be deduced as follows:

$$\max(w \times h) \quad (17)$$

$$\text{s.t. } \begin{cases} g_x = \{x_i - w/2 + (w/10)j, j = 1, 2, \dots, 10\}, i = 1, 2, \dots, \xi \\ g_y = \{y_i - h/2 + (h/10)j, j = 1, 2, \dots, 10\} \\ \text{point}(g_x, g_y) \in C, \text{ and } w, h \geq 0 \\ w \leq (\max(x_i) - \min(x_i)), h \leq (\max(y_i) - \min(y_i)) \end{cases} \quad (18)$$

where w and h are the estimated lengths along the X and Y axes, respectively.

In addition, the central coordinate of the circle-like or rectangle-like damage can also be calculated, which can correct the damage location $P^+(x_e, y_e)$ shown in subsection 2.1. In this case, the location and size of damage can be monitored simultaneously, thereby providing quantitative information for damage assessment.

3. Experiments and analysis

3.1. Experimental verification on a curved stiffened composite panel

A curved stiffened CFRP panel with a dimension of 1000 mm × 1000 mm × 3 mm and a curvature radius of 2000 mm is chosen as a specimen

to validate the proposed method. The CFRP panel is made of 15 layers of carbon fiber woven cloth using the Liquid Composite Molding process, and each layer can be considered as a quasi-isotropic laminate. Five U-shaped transverse stiffeners with the same dimensions of 640 mm × 50 mm × 2 mm, and two rectangular longitudinal stiffeners with the same dimensions of 740 mm × 30 mm × 6 mm are co-cured with the panel.

Considering that the preponderance of flexibility, electrically stabilized and apt for complex structures, sensor layers with embedded PZT sensor networks were surface-mounted on the monitored region using Hysol EA 9396 adhesive. A total of 36 manufactured identical PZT-5As were utilized as actuators or sensors. Each PZT has a diameter of 8 mm and a thickness of 0.48 mm.

3.1.1. Experimental setup

The experimental setup is shown in Fig. 4. The multi-channel switch system developed by the authors' group was used for Lamb wave exciting and receiving. The monitoring system includes a 128-channel switch system with a size of 223 mm × 201 mm × 49 mm and a host system with a size of 300 mm × 226 mm × 50 mm. The main technical indicators of the equipment are shown in Table 1. Five-peak sinusoidal waves were employed as driving signals and fed into PZT actuators to excite the monitored region. The adjacent sensors received the stress waves spreading via the stiffened plate.

The sensor layout is shown in Fig. 5. A path network composed of 190 actuator-sensor paths was established, and fourteen representative sensing paths were shown as the grey lines in Fig. 5(b). The peak-to-peak voltage, gain, sampling rate, sampling point, and sampling numbers of the output signal for representative paths are displayed in Table 2. Path parameters setting of other monitoring areas were set up in the same way. The constructed path network could locate any position of interest within the monitored region theoretically.

3.1.2. Damage evaluation

To verify the proposed theory, a kind of solid adhesive tape with different shapes and sizes as simulated damages were bonded on the surface of the CFRP panel. Sixteen artificial damage cases with thicknesses of 2 mm at different positions and sizes are illustrated in Table 3. The representative damage scenarios including circle-like damages (artificial damage cases 1–12 in Table 3) and rectangle-like damages (cases 13–16) with different characteristics were carried out for experimental investigation.

Guided wave signals were captured experimentally in both pristine benchmark and damaged status (before and after the artificial damage

Table 1
Monitoring equipment technical indicators.

Technical Parameter	Value
Excitation Frequency Range	10 kHz–1000 kHz
Conversion Rates	48 MHz
Output Voltage Range	Min: ±10 V Max: ±60 V
Memory	32,000 Samples
Sampling Rates	6,12,24,48 MHz/s
Resolution	12-bit
ADC Range	±1V
Gain Adjustment Range	10 dB–40 dB, step: 1 dB

was introduced). And the initial threshold value k_0 of boundary constraint for all damage cases is set as 0.8. The detailed damage localization and quantification results of the stiffened CFRP panel are listed in Table 3, in which symbol ϕ stands for diameter, and symbols w and h are denoted as the damage lengths along the X and Y axes, respectively.

The localization errors are calculated by the Euclidean distances between the localization results and actual damage locations. The quantitative errors are obtained by the absolute deviations between the estimated sizes and actual damage sizes. From Table 3, it can be found that accurate locations and size estimations can be attained whether the damages of different sizes or shapes are located in the internal or marginal areas. The average localization error is 7.72 mm, the average diameter estimation error of circle-like damages is 2.30 mm, and the maximum edge length estimation error of rectangle-like damage is less than 5 mm, thereby verifying the performance of the proposed technique.

A detailed comparison of searching capability between the LM approach and the improved LM (QLMC) approach is researched. Fig. 6 shows the contour maps of searching trajectories using the two algorithms with the same initially guessed locations. It can be seen that the optimal solution obtained by the improved algorithm is closer to the actual damage than the conventional LM method. Diagnostic localization images of the different damage situations using the proposed QLMC method are given in Fig. 7. The non-blue region indicates the effectuate constrained region Ω of each damage. And then a set of nonlinear equations for the constrained sensor network is constructed. The green and red dots display the estimated and actual locations of the damages. It can be indicated that the identified locations are approximately close to the real ones. Results prove that all damages can be accurately located by the proposed algorithm. However, it is also found that a higher error

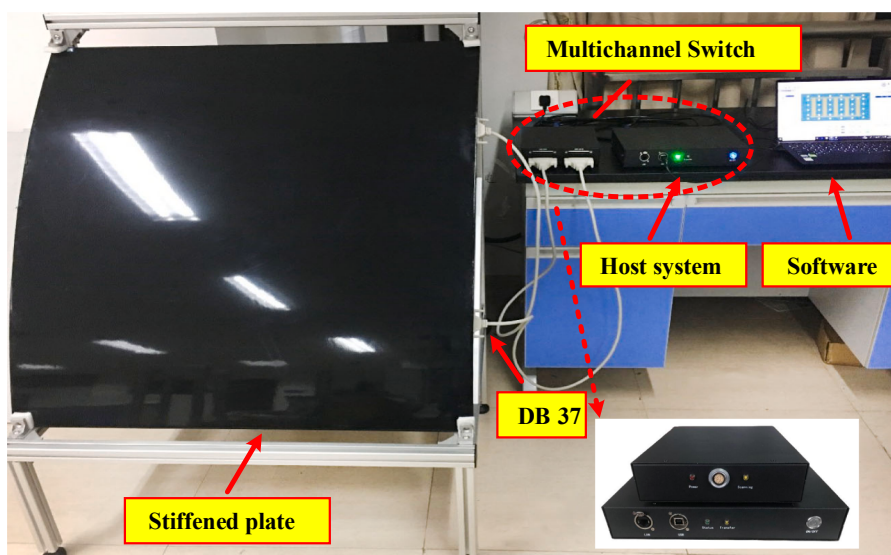


Fig. 4. Experimental setup for a curved stiffened CFRP panel.

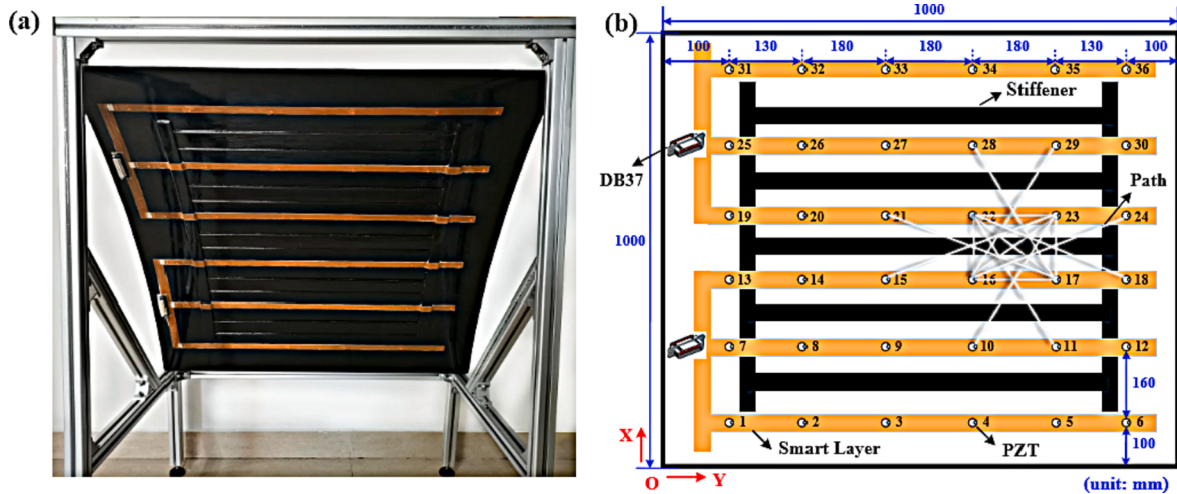


Fig. 5. Sensors layout: (a) CFRP panel with sensor layers installed; (b) sensor layout and sensing paths.

Table 2

Signal parameter setting of representative sensing paths for a curved stiffened CFRP panel.

Signal definition						Sampling rate	Sampling points	Sampling number
Actuator	Sensor	Signal type	Frequency (kHz)	Amplitude (V)	Gain (dB)			
17	16	Burst5	55	55	30	12,000,000	12,000	3
16	22		35	55	30			
23	17		40	60	30			
16	23		50	60	35			
22	17		35	60	30			
22	23		45	55	30			
10	23		30	60	40			
22	11		30	60	40			
15	23		30	60	40			
16	24		40	60	40			
16	29		30	60	40			
17	21		50	60	40			
28	17		30	60	40			
18	22		45	60	40			

Table 3

Damage localization and size quantification results for a curved stiffened CFRP panel (unit: mm).

No.	Damage centre	Identified centre	Localization error	Damage size	Identified size	Size error
1	(420, 585)	(419.70, 581.21)	3.80	Φ14	Φ14.17	0.17
2	(420, 585)	(422.50, 583.31)	3.02	Φ16	Φ13.08	2.92
3	(340, 90)	(331.16, 103.74)	16.34	Φ20	Φ18.36	1.64
4	(302, 400)	(302.54, 407.99)	8.01	Φ16	Φ18.16	2.16
5	(160, 820)	(150.23, 805.16)	17.76	Φ18	Φ14.74	3.26
6	(700, 270)	(701.84, 258.00)	12.14	Φ15	Φ11.94	3.06
7	(700, 270)	(705.00, 266.00)	6.40	Φ20	Φ19.45	0.55
8	(700, 270)	(692.80, 256.54)	15.26	Φ30	Φ26.43	3.57
9	(660, 670)	(659.91, 656.85)	13.15	Φ15	Φ17.02	2.02
10	(660, 670)	(649.19, 673.00)	11.22	Φ25	Φ21.15	3.85
11	(495, 466)	(492.58, 467.58)	2.89	Φ18	Φ16.79	1.21
12	(495, 466)	(495.82, 468.34)	2.48	Φ20	Φ16.86	3.14
13	(225, 225)	(225.73, 227.34)	2.45	h:13,w:13	h:11.5,w:12	h:1.5,w:1
14	(225, 225)	(220.71, 224.64)	4.30	h:20,w:20	h:16,w:17.6	h:4,w:2.4
15	(245, 185)	(245.98, 183.74)	1.60	h:13,w:13	h:14,w:15.8	h:1,w:2.8
16	(245, 185)	(244.43, 182.43)	2.63	h:20,w:20	h:15,w:20	h:5,w:0

exists in positions (340, 90) and (160, 820) which located on or adjacent to the stiffeners. This observation is probably attributable to the fact that the more sophisticated dispersive and mode coupling behaviors of Lamb wave signals near the stiffeners or boundaries, which induces inaccuracies in measuring the delay times T_{ij}^{TH} , and subsequently results in the large positioning errors.

The quantitative assessment results of damages with different sizes

and shapes are depicted in Fig. 8 for method verification visually. The damage reflection points (green asterisk) were calculated by searching the shortest distance between elliptical loci and the estimated damage position solved by the QLMC algorithm. Although a great majority of reflection points are close to the damage periphery, certain points still exist relevant to noise positioned away from the actual damage periphery. Thus, a singular elliptical loci removal scheme shown in

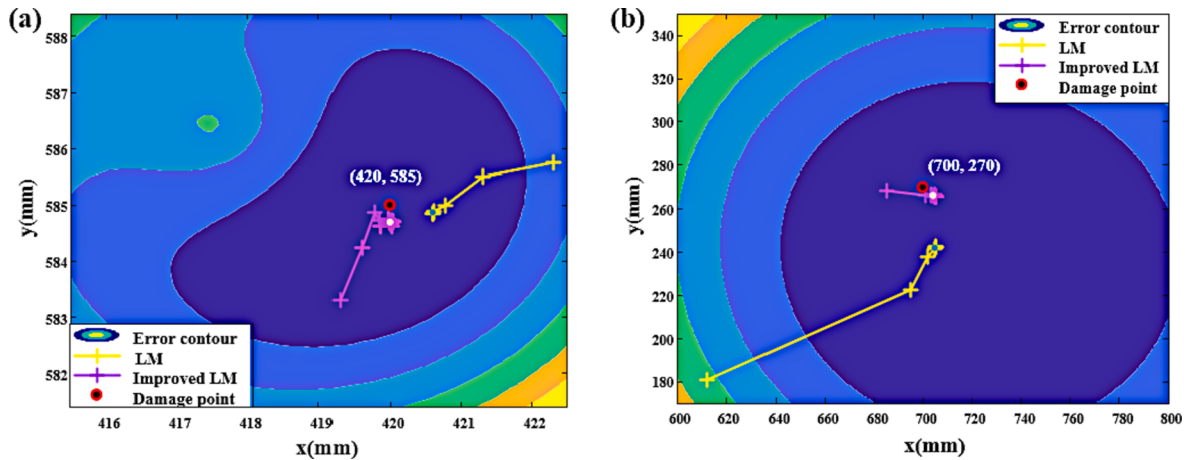


Fig. 6. Contour maps of the searching trajectories using the LM method and the improved LM (QLMC) method.

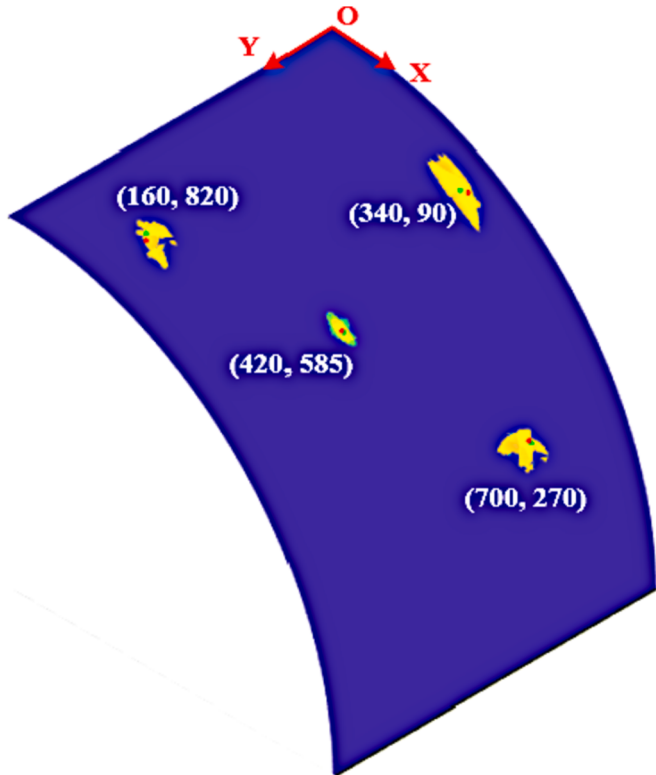


Fig. 7. Localization results using QLMC algorithm for the curved stiffened composite panel (unit: mm). (Green dot: identified position, red dot: actual position).

subsection 2.2.1 was utilized to separate the correctly positioned points on the damage periphery from those associated with noise. The selected points are highlighted as cyan dots in Fig. 8. Finally, by determining the corresponding convex hulls of selected points and calculating the maximum inscribed n -polygon, the approximate shapes and sizes of the damages were attained. The red and yellow lines display the estimated and actual damage size and shape. Comparing the two, it is evident that all the estimated damage centers and sizes agree satisfactorily with the actual ones. The damage evaluation results further substantiated that the proposed method is capable of pinpointing both location and size of the damage in the complex composite structures.

3.2. Experimental verification on circular through-thickness hole

In this section, as shown in Fig. 9(a), a real damage evaluation (i.e. circular through-thickness hole) in a CFRP panel with a dimension of 450 mm \times 450 mm \times 3 mm is further performed to demonstrate the capability of the developed technique. The composite laminates consist of six layers in a $[0^\circ/90^\circ]_3$ stacking sequence. Similar to subsection 3.1, four sensor layers with embedded PZTs sensor networks were surface-mounted on the CFRP panel using Hysol EA 9396 adhesive. And 16 manufactured identical PZT-5As were employed as actuators or sensors. The PZT type is identical with the one used in subsection 3.1, the diameter of the PZT sensor is 8 mm and the thickness is 0.48 mm. The sensor layout is shown in Fig. 9(b). A total of 66 actuator-sensor paths were constructed, the gray lines shown in Fig. 9(b) represent the representative sensing paths. A five-peak sinusoidal wave enclosed in a Hanning window at a central frequency of 80 kHz was excited and received at a sampling rate of 12 MHz. The peak-to-peak voltage and gain of the output signal were set as 60 V and 20 dB respectively. The responses of associated guided wave signals were logged by the multi-channel switch system mentioned in subsection 3.1.

In Fig. 9(a), four damage cases of different positions (① (320, 245), ② (147, 245), ③ (340, 185), and ④ (127, 185)) were carried out in the experiments, which included four circular through-thickness holes with the diameters of 12 mm. The holes were introduced by a Drilling machine. Responses of the associated active Lamb wave signals were recorded at each hole diameter of 5 mm, 8 mm, 10 mm, and 12 mm, respectively. The Lamb wave signals were captured experimentally in both pristine benchmark and damaged status (before and after the hole damage propagation was introduced). For example, the scattering signals subjected to different hole diameters at position (320, 245) are shown in Fig. 10. It is demonstrated that the amplitudes of scattering signals increase with the progressive incremental hole diameters, which is capable of commendably reflecting the damage propagation behavior.

The initial threshold value k_0 of boundary constraint for all damage cases is set as 0.8. Table 4 displays the detailed damage localization and quantification results of the four damage cases. It is evident that the identified damage centers tally commendably with that of the actual damage, the maximum localization error is 12.48 mm, and the maximum size estimation error is 2.08 mm. In addition, the results show that the average positioning and quantitative errors in all damage cases are 7.13 mm and 1.13 mm respectively, which are within the acceptable accuracy range. For visually authenticating the accuracy of the proposed method, Fig. 11 exhibits a stem3 graph of errors for four through-thickness holes at different locations and sizes. It can be demonstrated that the damage localization and quantification are achieved with minor estimated errors.

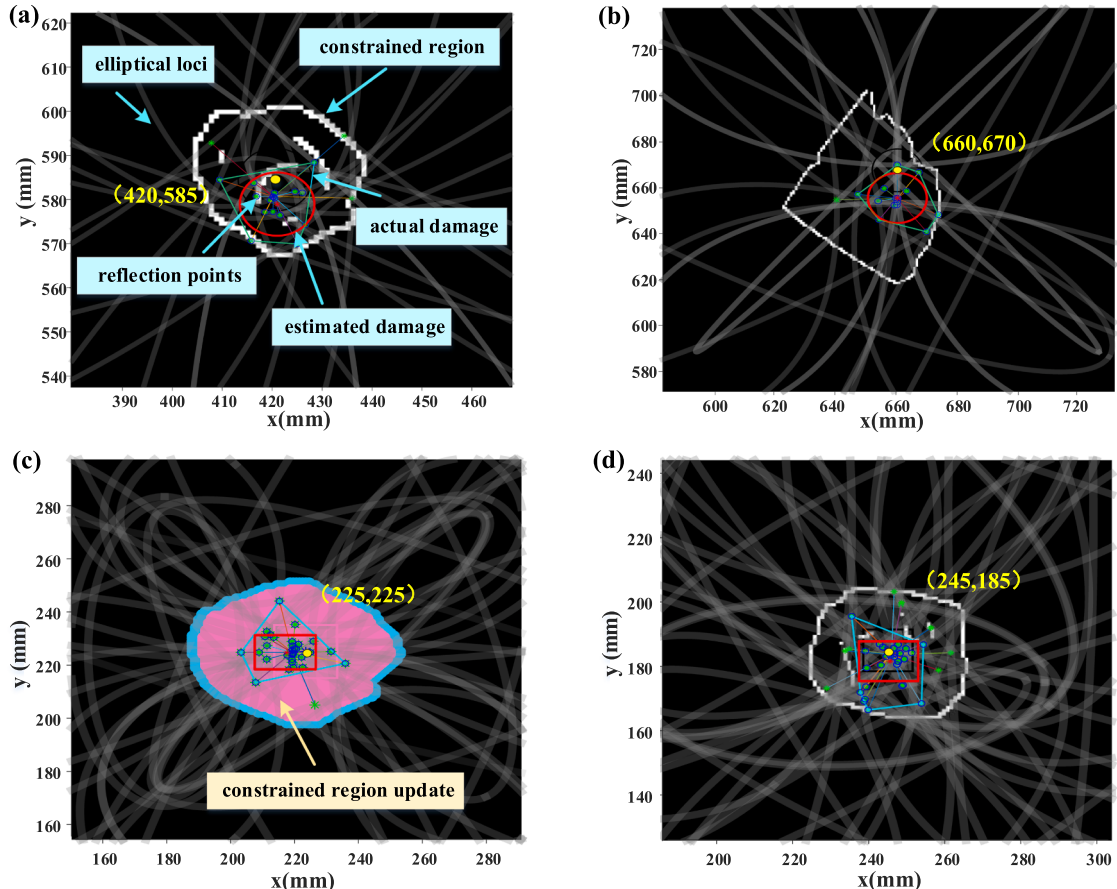


Fig. 8. Estimated (red line) and actual (yellow line) damage quantitative comparison: (a) damage center (420, 585) and $\Phi = 14$ mm; (b) damage center (660, 670) and $\Phi = 15$ mm; (c) damage center (225, 225) and $h = 20$ mm, $w = 20$ mm; (d) damage center (245, 185) and $h = 13$ mm, $w = 13$ mm.

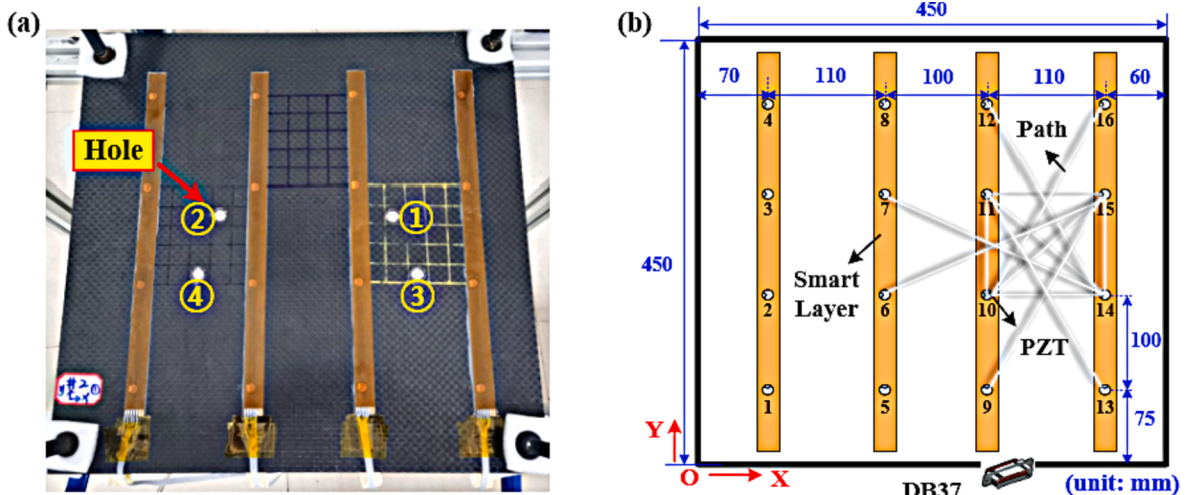


Fig. 9. Sensors layout: (a) CFRP panel with four real damage; (b) sensor layout and sensing paths.

Fig. 12 exhibits the quantitative damage assessment results of the four through-thickness holes with different positions at hole diameter $\Phi = 12$ mm. The proposed technique highlights the hole location and size in a large panel area. It is evident that all the identified locations of holes are nearby the actual positions, and the estimated sizes are also approximately close to the actual ones. The results further validate the feasibility of applying the proposed technique for damage evaluation.

From Table 4 and Fig. 11, it can also be indicated that the results of

through-hole diagnostic evaluation with smaller estimated errors than that of the curved stiffened CFRP panel mentioned in subsection 3.1.2. The discrepancies may result from that artificial damages with a kind of solid adhesive tape are easily polluted by the environment, resulting in ineluctable misleading wave scattering sources. On the other hand, especially for a more complex structure such as stiffened and curved CFRP panel, the complicated Lamb wave propagation characteristics would seriously affect the accuracy of damage evaluation. Without loss

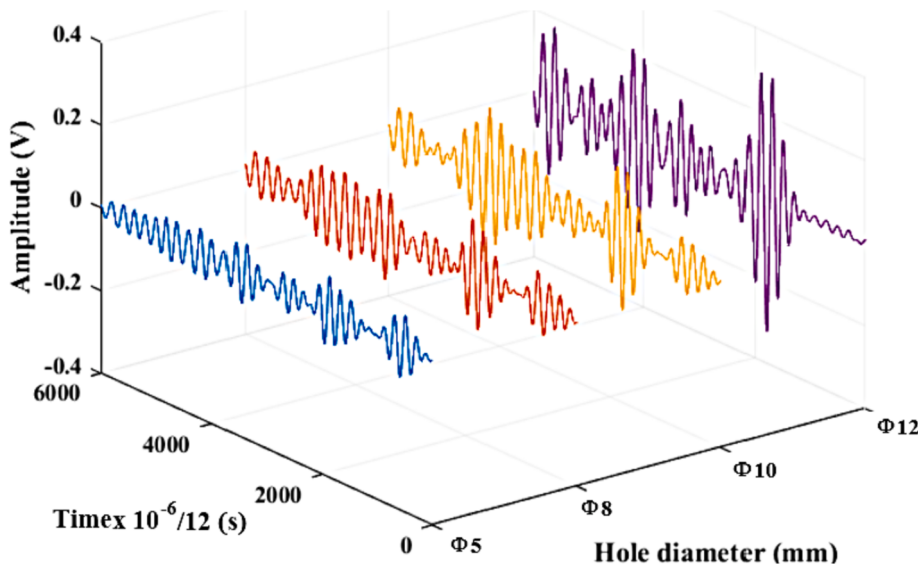


Fig. 10. Scattering signals subjected to different hole diameters at position (320, 245).

Table 4

Damage localization and size quantification results for circular through-thickness holes (unit: mm).

No.	Damage centre	Identified centre	Localization error	Damage size	Identified size	Size error
1	(320, 245)	(317.08, 241.64)	4.45	Φ 5	Φ 3.94	1.06
2	(320, 245)	(316.74, 246.61)	3.63	Φ 8	Φ 7.24	0.76
3	(320, 245)	(315.86, 247.17)	4.67	Φ 10	Φ 9.83	0.17
4	(320, 245)	(312.60, 253.38)	11.18	Φ 12	Φ 13.43	1.43
5	(147, 245)	(148.62, 247.48)	2.97	Φ 5	Φ 6.40	1.40
6	(147, 245)	(148.90, 250.04)	5.39	Φ 8	Φ 9.66	1.66
7	(147, 245)	(146.95, 252.72)	7.72	Φ 10	Φ 10.08	0.08
8	(147, 245)	(154.14, 250.26)	8.87	Φ 12	Φ 12.58	0.58
9	(340, 185)	(331.29, 186.00)	8.76	Φ 5	Φ 6.88	1.88
10	(340, 185)	(333.38, 184.82)	6.62	Φ 8	Φ 8.59	0.59
11	(340, 185)	(328.97, 190.84)	12.48	Φ 10	Φ 11.71	1.71
12	(340, 185)	(333.58, 185.36)	6.43	Φ 12	Φ 9.92	2.08
13	(127, 185)	(129.23, 179.64)	5.80	Φ 5	Φ 6.14	1.14
14	(127, 185)	(132.33, 177.80)	8.96	Φ 8	Φ 6.82	1.18
15	(127, 185)	(135.45, 181.80)	9.04	Φ 10	Φ 9.18	0.82
16	(127, 185)	(129.39, 191.75)	7.16	Φ 12	Φ 10.44	1.56

of generality, this work cites the damage localization and quantification methods in the quasi-isotropic composite laminates as an exemplification, whereas the fundamental research thinking can be expanded to other composite structures with different layouts or isotropic material structures, and also can obtain high-precision damage assessment results expectedly. Nevertheless, for the damage evaluation of the more complex and larger-scale structures, the more sophisticated dispersive and mode coupling effects would make the signal interpretation problematic, which will be investigated in future work.

4. Conclusion

An innovative damage monitoring method based on the Lamb wave is proposed for large-scale complicated composite laminates. Experiments on two large-scale composite panels with multiple damage cases are conducted to verify the proposed method. Based on the analytical and experimental investigations, the conclusions are highlighted as follows:

- The proposed technique is capable of determining both location and size of the damages in complicated composite structures. The damage centers and quantitative sizes are estimated well for all damage cases.

- For a curved stiffened CFRP panel with a sensor spacing of 180 mm (but reduced to 160 mm and 130 mm when passing through the transverse stiffener and longitudinal stiffener respectively), the average localization error is 7.72 mm, the average diameter estimation error of circle-like damage is 2.30 mm, and the maximum edge length estimation error of rectangle-like damage is less than 5 mm. For all real through-thickness hole damage cases, the average positioning and quantitative errors are 7.13 mm and 1.13 mm respectively with a sensor spacing of 100 mm.
- The implementation of the proposed methodologies is comparatively simple and straightforward for efficient damage detection in composite structures, which makes it ideal for on-line monitoring.
- The proposed damage monitoring method was verified in the quasi-isotropic composite laminates, whereas the fundamental research thinking can be expanded to other composite structures with different layouts or isotropic material structures, and the expected high-precision estimation results would also be obtained. However, there still remains some challenges for more complex and larger-scale structures, such as the more sophisticated dispersive and mode coupling effects would make the signal interpretation problematic, and the larger sensor networks are required to cover the entire monitoring area would increase the difficulty of signal processing in SHM.

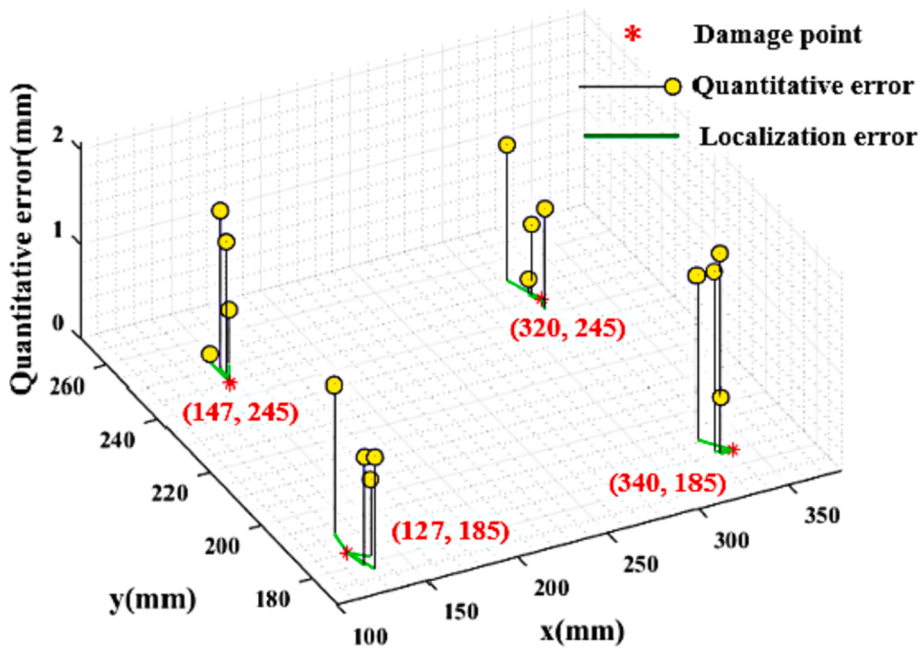


Fig. 11. A stem3 graph of errors for four through-thickness holes at different locations and sizes.

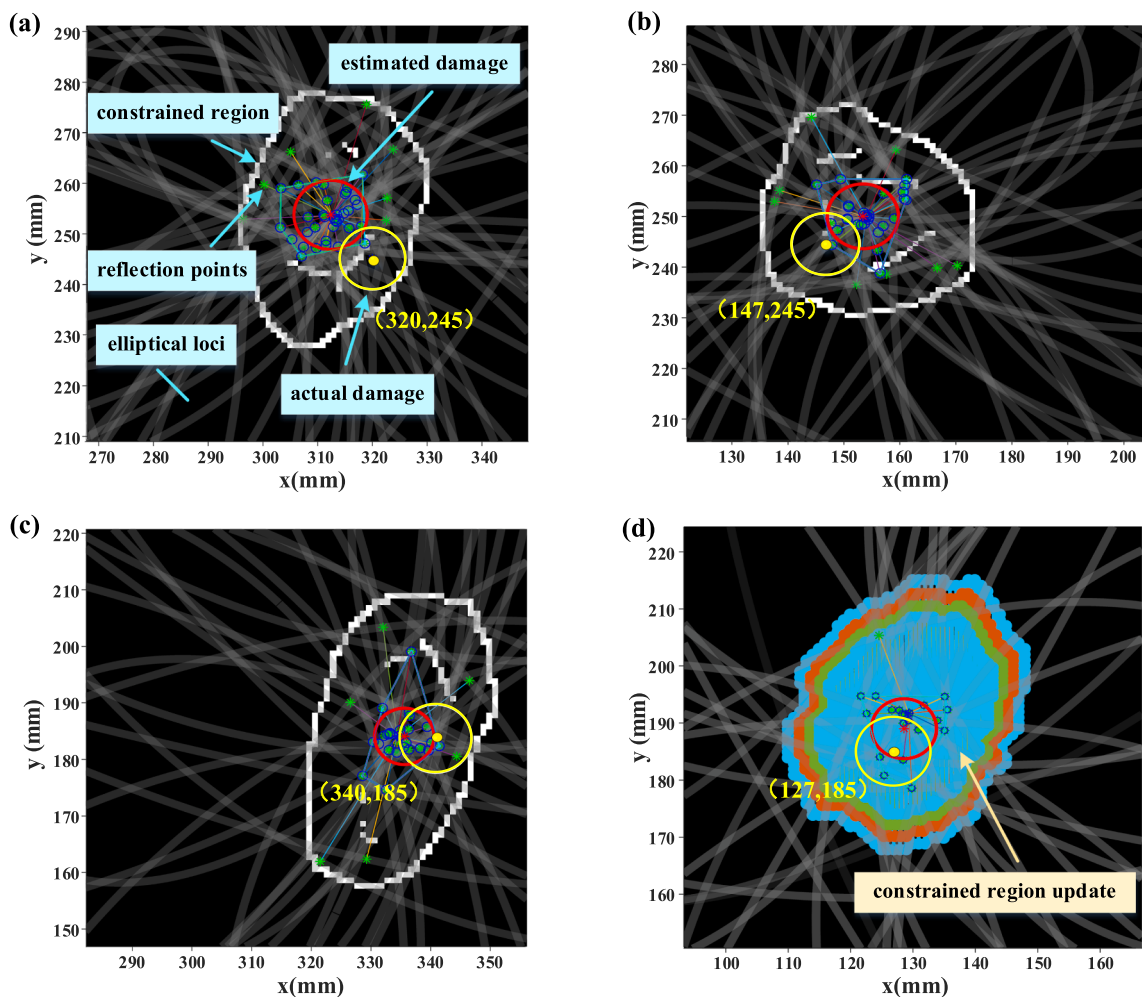


Fig. 12. Estimated (red line) and actual (yellow line) damage quantitative comparison with hole diameter $\Phi = 12$ mm: (a) damage center (320, 245); (b) damage center (147, 245); (c) damage center (340, 185); (d) damage center (127, 185).

CRediT authorship contribution statement

Xianping Zeng: Conceptualization, Methodology, Data curation, Validation, Formal analysis, Writing – original draft, Writing – review & editing. **Xiao Liu:** Data curation, Writing – review & editing. **Jiajia Yan:** Supervision. **Yinghong Yu:** Data curation. **Bowen Zhao:** Data curation. **Xinlin Qing:** Methodology, Project administration, Writing – review & editing.

Declaration of Competing Interest

The authors declare that they have no known competing financial interests or personal relationships that could have appeared to influence the work reported in this paper.

Acknowledgement

This research was supported by National Natural Science Foundation of China (Grant Nos. U2141245, 11972314, 11472308).

References

- [1] Bajpai P. Applications of carbon fiber/carbon fiber-reinforced plastic/recycled carbon fiber-reinforced polymers. Carbon Fiber (Second Edition) 2021;139–55.
- [2] Sato M, Hasegawa K, Koyanagi J, Higuchi R, Ishida Y. Residual strength prediction for unidirectional CFRP using a nonlinear viscoelastic constitutive equation considering entropy damage. Compos A Appl Sci Manuf 2021;141:106178.
- [3] Memmolo V, Monaco E, Boffa ND, Maio L, Ricci F. Guided wave propagation and scattering for structural health monitoring of stiffened composites. Compos Struct 2018;184:568–80.
- [4] Qing X, Li W, Wang Y, Sun H. Piezoelectric transducer-based structural health monitoring for aircraft applications. Sensors 2019;19(3):545.
- [5] Huang S, Zhang Yu, Wang S, Zhao W. Multi-mode electromagnetic ultrasonic Lamb wave tomography imaging for variable-depth defects in metal plates. Sensors 2016;16(5):628.
- [6] Agrahari JK, Kapuria S. Active detection of block mass and notch-type damages in metallic plates using refined time-reversed Lamb wave technique. Struct Control and Health Monitoring 2018;25(2):e2064.
- [7] Wu Z, Liu K, Wang Y, Zheng Y. Validation and evaluation of damage identification using probability-based diagnostic imaging on a stiffened composite panel. J Intell Mater Syst Struct 2015;26(16):2181–95.
- [8] Sharif-Khodaei Z, Aliabadi MH. Assessment of delay-and-sum algorithms for damage detection in aluminium and composite plates. Smart Mater Struct 2014;23(7):075007.
- [9] Liu K, Ma S, Wu Z, Zheng Y, Qu X, Wang Y, et al. A novel probability-based diagnostic imaging with weight compensation for damage localization using guided waves. Struct Health Monitoring 2016;15(2):162–73.
- [10] Shan S, Qiu J, Zhang C, Ji H, Cheng Li. Multi-damage localization on large complex structures through an extended delay-and-sum based method. Struct Health Monitoring 2016;15(1):50–64.
- [11] Xu C, Yang Z, Tian S, Chen X. Lamb wave inspection for composite laminates using a combined method of sparse reconstruction and delay-and-sum. Compos Struct 2019;223:110973.
- [12] Giridhara G, Rathod VT, Naik S, Roy Mahapatra D, Gopalakrishnan S. Rapid localization of damage using a circular sensor array and Lamb wave based triangulation. Mech Syst Sig Process 2010;24(8):2929–46.
- [13] Zeng L, Huang L, Lin J. Damage imaging of composite structures using multipath scattering Lamb waves. Compos Struct 2019;216:331–9.
- [14] Ciampa F, Meo M. A new algorithm for acoustic emission localization and flexural group velocity determination in anisotropic structures. Compos A Appl Sci Manuf 2010;41(12):1777–86.
- [15] Cantero-Chinchilla S, Chiachio J, Chiachio M, Chronopoulos D, Jones A. A robust Bayesian methodology for damage localization in plate-like structures using ultrasonic guided-waves. Mech Syst Sig Process 2019;122:192–205.
- [16] Yan G. A particle filter method for damage location in plate-like structures by using Lamb waves. Struct Control and Health Monitoring 2014;21(6):847–67.
- [17] Campeiro LM, Budoya DE, Baptista FG. Lamb wave inspection using piezoelectric diaphragms: an initial feasibility study. Sens Actuators A Phys 2021;331(3):112859.
- [18] Yelve N, Mitra M, Mujumdar P. Spectral damage index for estimation of breathing crack depth in an aluminum plate using nonlinear Lamb wave. Struct Control and Health Monitoring 2014;21(5):833–46.
- [19] Yang J, He J, Guan X, Wang D, Chen H, Zhang W, et al. A probabilistic crack size quantification method using in-situ Lamb wave test and Bayesian updating. Mech Syst Sig Process 2016;78:118–33.
- [20] Hu N, Cai Y, Zhu G, Tsuji C, Liu Y, Alamusi, et al. Characterization of damage size in metallic plates using Lamb waves. Struct Health Monitoring 2012;11(2):125–37.
- [21] Qiu L, Liu M, Qing X, Yuan S. A quantitative multidamage monitoring method for large-scale complex composite. Struct Health Monitoring 2013;12(3):183–96.
- [22] Zhang S, Li CM, Ye W. Damage localization in plate-like structures using time-varying feature and one-dimensional convolutional neural network. Mech Syst Sig Process 2021;147:107107.
- [23] Wu J, Xu X, Liu C, Deng C, Shao X. Lamb wave-based damage detection of composite structures using deep convolutional neural network and continuous wavelet transform. Compos Struct 2021;276:114590.
- [24] Liu H, Liu S, Liu Z, Mrad N, Milani AS. Data-driven approaches for characterization of delamination damage in composite materials. IEEE Trans Ind Electron 2021;68(3):2532–42.
- [25] Gorgin R, Wu Z, Gao D, Wang Y. Damage size characterization algorithm for active structural health monitoring using the A0 mode of Lamb waves. Smart Mater Struct 2014;23(3):035015.
- [26] Lu G, Li Y, Zhou M, Feng Q, Song G. Detecting damage size and shape in a plate structure using PZT transducer array. J Aerosp Eng 2018;31(5):04018075.
- [27] Gao F, Zeng L, Lin J, Shao Y. Damage assessment in composite laminates via broadband Lamb wave. Ultrasonics 2018;86:49–58.
- [28] Hameed MS, Li Z. Transverse damage localization and quantitative size estimation for composite laminates based on Lamb waves. IEEE Access 2019;7:174859–72.
- [29] Qing X, Liao Y, Wang Y, et al. Machine learning based quantitative damage monitoring of composite structure. International Journal of Smart and Nano Materials, 2022, DOI: 10.1080/19475411.2022.2054878.
- [30] Kanizawa C, Yamashita N, Fukushima M. Levenberg-Marquardt methods with strong local convergence properties for solving nonlinear equations with convex constraints. J Comput Appl Math 2004;172(2):375–97.
- [31] Soleimanpour-Moghadam M, Nezamabadi-Pour H, Farsangi MM. A quantum inspired gravitational search algorithm for numerical function optimization. Inf Sci 2014;267:83–100.